



Lithiation of Silicon Nanoclusters

Andreas Pedersen,^{*} Michael Bieri, and Mathieu Luisier

*Integrated Systems Laboratory, Department of Electrical Engineering and Information Technology,
ETH Zurich, Gloriastrasse 35, 8092 Zurich, Switzerland*

Laurent Pizzagalli

*Institut P', CNRS UPR 3346, Université de Poitiers, SP2MI, BP 30179, Boulevard Marie et Pierre Curie,
86962 Futuroscope Chasseneuil Cedex, France*

(Received 19 January 2017; revised manuscript received 21 March 2017; published 16 May 2017)

In this paper, we investigate the lithiation of pristine amorphous silicon nanoclusters with diameters from 0.8 to 1.4 nm using first-principles molecular dynamics. It is found that this process occurs in two stages. In the first one, Li atoms accumulate at the surface of the nanocluster. A transfer of electrons from Li to the Si atoms takes place, which is accompanied by moderate structural changes. At a given Li coverage threshold that is related to the nanoparticle size, it becomes energetically favorable for any additional Li atoms to penetrate into the nanoparticle. Our results suggest that the driving force for this transition is the increasing electrostatic repulsion between positively charged surface Li ions. Beyond the threshold a second lithiation stage starts where the nanocluster is progressively filled with Li atoms. This leads to significant structural changes, but no sign of fracture is observed during the first lithiation cycle, suggesting that the amorphous silicon cluster remains intact at this size.

DOI: [10.1103/PhysRevApplied.7.054012](https://doi.org/10.1103/PhysRevApplied.7.054012)

I. INTRODUCTION

Lithium-ion batteries have become essential components in most portable electronic devices. To improve the battery performance in terms of energy density and cycle life, a tremendous research effort has been dedicated to the replacement of graphite by other anode materials [1–5]. Among these, Si-based systems have probably been the most scrutinized, both experimentally and theoretically, due to the abundance and low price of Si. Furthermore, Si is characterized by one of the highest known maximal theoretical specific capacities, 4200 mA h g^{-1} [3]. However, the utilization of Si-based anodes in Li-ion batteries is severely hampered by several effects, especially dramatic volume changes during lithiation and delithiation [6], which leads to a fast capacity fade at prolonged cycling. This unacceptable issue currently hinders a full commercialization of Si-based batteries. To resolve it, different strategies have been proposed, involving size reduction, geometry optimization, and material structuring [7–9]. It is particularly noteworthy that several studies revealed that decreasing the characteristic size to the nanoscale could prevent the deterioration of the anode integrity [10–14]. For instance, Liu and co-workers found that crystalline Si nanoparticles with diameters below 150 nm do not exhibit fractures, thus preserving the intrinsic properties of the material [15]. A similar behavior has been demonstrated for amorphous-Si (*a*-Si) nanoparticles with even larger sizes

reaching 870 nm [16]. These submicronic systems remain of sufficient size for bulk lithiation concepts to fully apply. In this size regime it is known that during the first cycle, the lithiation of crystalline or amorphous bulk Si occurs via a two-phase process [6,17]. Initially, a sharp interface separates lithiated and pristine Si and the displacement of this interface limits the whole process. In crystalline nanowires, the lithiation is observed to develop anisotropically because of mobility differences between possible interface orientations [18–21], leading to significant changes in morphology. Conversely, the lithiation of amorphous silicon nanostructures is isotropic. It is assumed that the reaction front motion is directly related to Si–Si bond weakening, which may be triggered by charge transfer from Li atoms into Si antibonding states, and to stress induced by the volume expansion of the lithiated phase [22–24]. Nevertheless, it is important to realize that for both crystalline and amorphous pristine Si, an amorphous phase results after the first (de)lithiation cycle and this amorphous phase remains during subsequent lithiation and delithiation iterations.

In recent works ultrasmall nanoparticles, i.e., with sizes smaller than 10 nm, have been identified as promising candidates for the capture of Li [12,13]. Impressive results have been achieved for the case of graphene-supported 3-nm Si nanoparticles [14]. In addition to a better mechanical stability, these also allow for improved transport properties due to shorter paths for Li ions and electrons. It is worth mentioning that for such small systems the bulk lithiation concepts are hardly applicable.

^{*}andped10@gmail.com

In fact, there is not enough volume to form a well-defined lithiated-interface-pristine structure and the surface becomes a dominant actor at this scale. At present, there is still an obvious lack of knowledge regarding the lithiation of such small Si nanoparticles. Okamoto investigated the dynamical lithiation of a crystalline Si₃₅ cluster using first-principles calculations [25]. However, it is not clear whether a crystalline sample is representative for real systems at such reduced sizes where disordered structures are known to be favored. Theoretical investigations of disordered nanoparticles are typically more complicated than for crystalline ones since a huge number of possible configurations exist. Another difficulty is the need to use accurate first-principles calculations because the commonly used empirical interatomic potentials are not able to reproduce the quantum confinement effects that prevail at the nanoscale.

In this paper, we report on the study of the lithiation of ultrasmall *a*-Si nanoparticles investigated by an extensive set of *ab initio* density functional theory (DFT) calculations. The simulations reveal that lithiation occurs through two consecutive processes. First, the surface of the nanoparticles is progressively homogeneously covered with Li atoms until a critical level is reached. Beyond this threshold, it becomes energetically favorable for Li atoms to penetrate into the nanoparticle, leading to significant structural modifications. In particular, it will be shown that despite a strong volume expansion, the nanoparticles keep their integrity even at high lithiation levels during the initial lithiation process. This supports the experimental observations that *a*-Si nanoclusters (NCs) could be suited as the active component of high-performance anode material in Li-ion batteries.

II. COMPUTATIONAL METHODS

A. Atomic interactions

Atomistic calculations are performed in the framework of DFT as implemented in the Vienna *ab initio* simulation package (VASP) [26,27]. The main priority is to sample the largest possible collection of configurations. Hence, the computational efficiency is maximized by applying the projector-augmented wave method [28] and a local-density approximation pseudopotential to determine the electronic density of the treated samples. Furthermore, the plane-wave basis is restricted to a moderate size using a cutoff of 184.3 eV. The electronic degrees of freedom are assumed converged when the change in energy falls below 10⁻⁵ eV. Finally, the *k*-point sampling contains only the Γ point, which is appropriate for isolated systems such as clusters. To validate the chosen simulation setup, the total energy of configurations at the shift in site preference (see next section) have been redetermined using a higher cutoff energy (307.1 eV) and the generalized gradient approximation to the exchange correlation functional with the

Perdew-Burke-Ernzerhof parametrization [29]. These additional calculations show that only marginal changes occur in the relative energy difference, when the two approaches are compared with each other.

B. Structures and dynamics

Three sizes of Si NCs consisting of either 40, 55, or 70 Si atoms are considered. This corresponds to a diameter ranging from 0.8 to 1.4 nm. The clusters are embedded within a cubic supercell of dimensions large enough to avoid spurious interactions with periodic replicas. A high priority is given to the determination of configurations with the lowest possible energy. This is the case since these are the ones that most likely are observed in an experiment at ambient temperature as stated by statistical physics. If a too-rapid quenching is undertaken the system tends to end up in a local minimum configuration situated close to the initial high-temperature structure. To alleviate this, a relatively slow cooling is undertaken, which will give the system time to surpass energy barriers and thereby settle down in a more optimal configuration. A representative low-energy configuration for each of the three pristine Si NCs is therefore obtained as follows. After an initial relaxation, thorough molecular-dynamics simulations (time step of 1 fs) are performed using a Nose-Hoover thermostat applying a down-ramping temperature profile: starting from a temperature of 1000 K, the system is cooled down to 300 K using a profile with steps at 750 and 500 K. During this annealing procedure the atomic configuration is frequently extracted and relaxed to determine the inherent structure, which allows one to inspect a large number of configurations. These local minimization runs are considered converged when the largest atomic force falls below 10⁻⁴ eV/Å. In most cases a temperature lowering causes a decrease in energy of the inherent structure. However, if this is not the case additional steps at the preceding higher temperature are conducted.

By applying this treatment on the three Si NCs it is clear that regardless of an initial structure being either ordered or amorphous, the resulting lowest-energy configuration is always a disordered nanoparticle with an approximate spherical shape, as shown in Fig. 1. This finding is in agreement with previous investigations of Si NCs [30,31] and the obtained pristine *a*-Si NCs serve as reference configurations to determine the effects of lithiation. Usually, the treatment corresponds to a 5-ps simulation, but rare cases require up to 32 ps. It should be mentioned that the accumulated grand total of *ab initio* molecular-dynamics iterations exceeds 1.1×10^6 when including the simulations of the lithiation processes, which corresponds to a total simulation time of 1.1 ns. This is required to typically let three candidate structures evolve per lithiation level, in certain cases up to six.

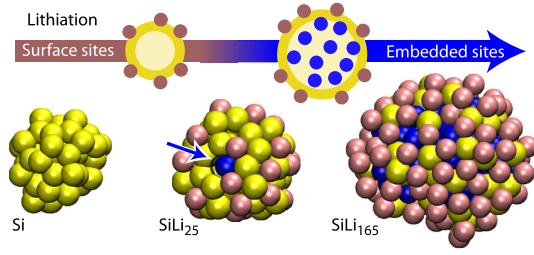


FIG. 1. Schematic and spacefill representations (yellow for Si atoms, pink and blue for surface and subsurface Li atoms, respectively) of the NC_{55} system before lithiation (left), at the threshold where the first Li atom (blue arrow) penetrates into the nanoparticle (center), and for a 300% lithiation (right).

C. Lithiation

To lithiate a Si cluster, neutral Li atoms are added to the configuration. This is done under the assumptions that the $(a\text{-Si}) + \text{Li}$ cluster remains charge neutral and that a captured positively charged Li ion instantly recombines with its missing electron, which is provided from an infinite reservoir. The energy gained by the electrode as Li is captured is a very important quantity that directly relates to the voltage profile. For the case of Li, where a single electron is transferred per ion, the change in voltage equals the change in energy divided by the charge of an electron. The average binding energy is determined according to the following expression:

$$E_b(x) = \frac{E_N - (E_{N-x} + xE_{\text{Li}})}{x}, \quad (1)$$

where the resulting average relative binding energy $E_b(x)$ is calculated for each of the x newly captured Li atoms; E_N is the total energy of the NC structure when N Li atoms are already present, and E_{Li} is the cohesive energy of a Li atom in a bcc bulk environment. This definition is equivalent to what has been proposed by Courtney *et al.* in Ref. [32]. From this expression it is clear that the computational task consists of rigorously determining the lowest-energy configuration for a given Li level.

III. RESULTS

A. Li site preference

The first series of simulations concerns the site preference for Li on Si NCs at varying lithiation levels. This site preference is determined by refining various systems starting from an initial configuration either having all Li atoms on the NC surface at random positions or with a single Li atom embedded into the core of the cluster. Elaborate lithiation protocols have been proposed for a -Si bulk [33] and crystalline-Si (c -Si) surfaces [34]. However, the computational requirement for the NC sizes studied here makes it feasible to use the earlier-described annealing procedure that allows for an unbiased determination of

low-energy configurations. In particular, with our procedure it can be established whether Li atoms prefer to stay on the surface or at sites embedded in the cluster at the thermodynamical equilibrium.

Numerous configurations have been tested for the lowest lithiation levels. These simulations reveal that the initial Li atoms always have a strong energetic preference of residing on the surface, while the NC core remains a Li-free environment. The surface site that offers the strongest binding to the lowest-energy pristine NC_{55} a -Si core is associated with an energy gain of -0.99 eV. As a second Li atom is introduced, the average energy gain reduces to -0.83 eV when the reference is the pristine NC ($x = 0$), whereas the relative gain for the newly added Li atom is only -0.67 eV when the reference is the NC already containing a single Li atom ($x = 1$).

As further Li atoms are introduced, the surface sites remain favored, which is a clear trend that continues up until a critical Li level is reached. In the case of NC_{40} , this threshold corresponds to the capture of 21 Li atoms that equals to a concentration ratio of 53%. In fact, the configurations with the lowest energy remain to have 20 Li atoms on the NC surface, while only a single Li atom enters an embedded side inside the nanoparticle. For NC_{55} (NC_{70}), the transition happens for 24 (25) Li atoms that correspond to a Li concentration ratio of 44% (36%). It appears that at these thresholds, the NC surface becomes saturated and additional Li atoms start to penetrate into subsurface sites. This hypothesis is supported by the correlation between the increasing Li thresholds and the NC size. However, no quantitative relation could be found between these values and the estimated NC surface areas, likely because of the limited set of sizes investigated here. Larger systems are expected to give a more consistent behavior but they are out of the reach of first-principles calculations.

B. Continuous lithiation

To get a better understanding of the shift in site preference for increasing lithiation, a second series of molecular-dynamics simulations is performed to investigate a single NC_{55} structure. These calculations follow the refinement technique mentioned above, but with a significantly different procedure for loading Li onto the cluster: (i) only a single pristine configuration is evolved and (ii) new Li atoms are always added on the surface of the most stable configuration obtained at the preceding lithiation level. This approach allows for an estimation of the upper limit for the lithiation threshold at which it is energetically favorable for a Li atom to enter the nanoparticle core by surpassing a negligible energy barrier. High lithiation levels are also studied in this series of calculations, with configurations containing 55, 110, and 165 Li atoms.

Figure 2(a) shows the total and relative change in energy as Li is captured (Li binding energy), the latter representing

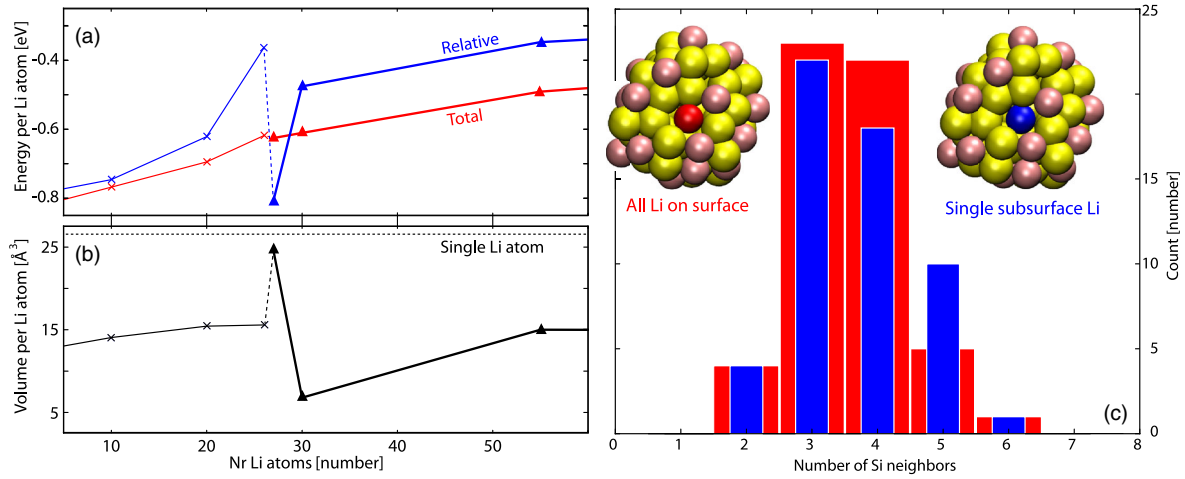


FIG. 2. (a) Li binding energy as a function of the lithiation level for NC_{55} . The red curve shows the total binding energy with respect to the initial pristine α -Si cluster, which also corresponds to the voltage profile. The blue curve is the relative binding energy, with the preceding configuration as a reference. (b) Volume expansion as a function of the lithiation level for NC_{55} . The black curve refers to the volume expansion per Li atom as compared to the preceding configuration. The dashed line segments mark the discontinuity occurring as the critical Li level is reached. (c) Changes in Si-Si coordination when one Li atom enters a subsurface site for NC_{55} carrying 27 Li atoms. Red bars correspond to the configuration before the event, and blue bars account for the configuration after. Insets are a spacefill representation where yellow and pink are Si and Li atoms, respectively, whereas red and blue represents the Li atom that enters a subsurface site.

the derivative of the former, as a function of the number of Li atoms for the NC_{55} structure. The energy gain follows a monotonic decrease at low Li levels, thus confirming that these simulations describe a continuous lithiation process without any significant structural changes of the α -Si host. However, a pronounced discontinuity occurs at 27 Li atoms. It corresponds to the Li level where a Li atom migrates from the surface to the NC core. Another interesting feature is the relatively fast decline in binding energy just before a subsurface site gets occupied. This indicates that Li atoms prior to this event are forced into surface sites of reduced binding up until it becomes energetically favorable to “crack” the α -Si surface shell. These findings are in agreement with our proposed hypothesis that the surface first reaches a Li-saturated state before Li atoms enter into subsurface sites. For the structures at the highest lithiation levels, not shown in the plot, the relative binding energy reduces from 0.26 eV/Li at 110 Li atoms down to 0.03 eV/Li at 165 Li atoms. An upper bound for a complete lithiation of the considered 55 α -Si cluster can therefore be deduced: it is equal to 165 Li atoms. Using this value as the maximum load level, the structures with 10 and 50 Li atoms correspond to 6% and 30% of the full load level, respectively. From the experimental results in Ref. [14] [see Fig. 3(c)], it can be seen that at similar load levels the open-circuit voltage changes from 0.7 to 0.4 V. Here, the computed reduction in total binding energy goes from 0.78 to 0.5 eV/Li, which can be directly converted into volts and appears to be within the expected range.

The shift in site preference takes place at 24 Li in the first series of calculations. It should be emphasized that the

difference between the two threshold Li levels, Li_{24} in the first MD series and Li_{27} in the second one, does not indicate uncertainty in the results, since these levels are achieved under widely different simulation conditions. In the first series, we actually compare the energy of different cluster configurations with either all Li atoms on the surface or with one Li placed inside the NC. The transition then occurs when a configuration with an embedded Li atom becomes thermodynamically favored as compared with structures where all Li atoms are on the surface, regardless of the energy barrier associated with the process where Li migrates into the α -Si core. In the second series, a single cluster is evolved and the loading of Li atoms is done by placing additional Li atoms on the surface of a low-energy configuration, thus mimicking a continuous lithiation process. As a consequence, the transition to a structure with one embedded Li site only takes place if the energy barrier for this event is sufficiently low for it to occur within the limited time scale of first-principles molecular-dynamics simulations.

To illustrate this point, the minimum energy path for the transition where one single Li enters into the NC core is calculated. The initial configuration is a structure with all Li on the surface, whereas the final one has one subsurface Li. This analysis is done for two different lithiation levels (20 and 27 Li atoms) and performed using the nudged elastic band (NEB) method [35]. The end-point configurations are extracted from the MD simulations and the band consists of five images generated by the image-dependent pair-potential method [36]. These NEB calculations are considered converged when the change in energy between two

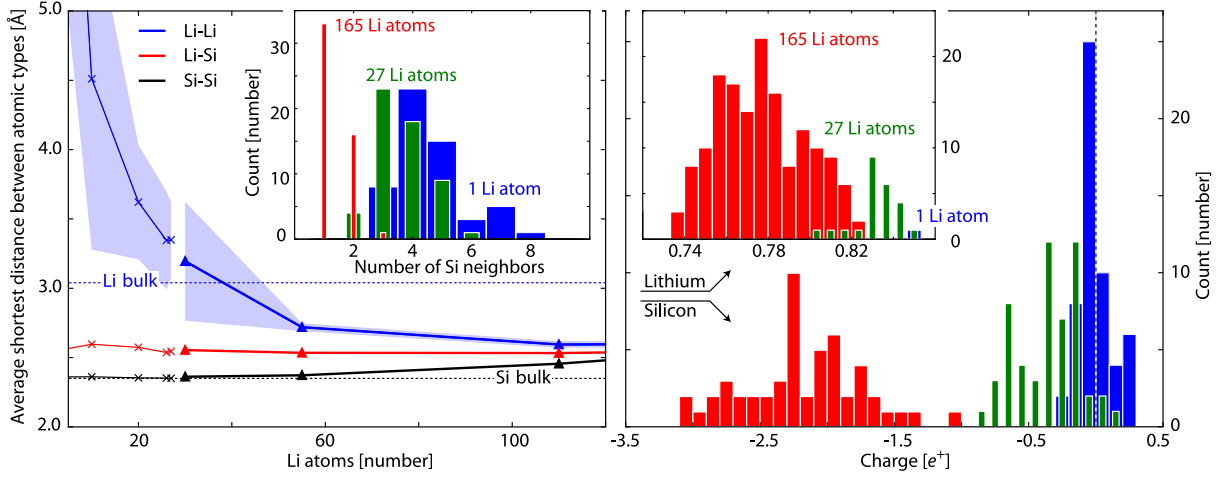


FIG. 3. Left panel: Average shortest pair distance as a function of the lithiation level for NC_{55} . Blue represents Li-Li pairs, red Si-Li pairs, and black Si-Si pairs. The blue-shaded area indicates the variance for the Li-Li pairs. The dashed lines indicate the bond length for Si (Li) in the diamond (bcc) phase. Crosses connected by thin line segments represent configurations where all Li are on the surface (≤ 26), whereas triangles and thick segments are configurations where some Li atoms have moved inside the cluster (≥ 27). The inset shows the Si-Si coordination for NC_{55} at different lithiation levels (blue bars for 1 single Li atom, green bars for 27 Li atoms, and red bars for 165 Li atoms). Right panel: Histogram of charge distributions on the Si atoms for NC_{55} at increasing lithiation levels, same color code as for Si-Si coordination. The inset represents the charge distribution on the Li atoms.

iterations becomes less than 10^{-3} eV. When being below the determined Li shift in site preference (20 Li atoms) the barrier is determined to be 115 meV, while the 27 Li atoms structure (above the threshold) exhibits a much-reduced energy barrier of 5 meV. Furthermore, only for the structure above the threshold level do the final configuration results in a significant energy decrease of 0.54 eV. The results obtained from these additional calculations further support the here-proposed picture that the NC surface is first progressively covered with Li atoms, until it reaches a saturated state for which it becomes energetically favorable for Li atoms to be incorporated into the core of the NC.

IV. ANALYSIS AND DISCUSSION

A deeper knowledge about the lithiation process can be gained by analyzing the ongoing structural changes and charge distribution for the series of simulations that represent a continuous lithiation process. To estimate the volume changes of a NC, we represent each of the Si and Li atoms as spheres with van der Waals radii of 2.10 and 1.85 Å, respectively. Following that, a triangular mesh is constructed to enclose these spheres and the volume of the resulting polyhedron is determined. Changes in the local atomic structure are investigated in terms of Si-Si coordination. This analysis is done using a pair cutoff distance of 2.80 Å, which corresponds to the minimum between the first and second neighbor peaks of the bulk *a*-Si radial-distribution function [37]. Finally, changes in charge distribution are also evaluated by attributing charge to individual atoms through a Bader analysis of the total electron density [38].

A. Volume and atomic structure

The volume variations are evaluated in a similar fashion as the energy in Eq. (1). The resulting volume expansion per Li atom is plotted in Fig. 2(b), while the total volume expansions are reported in Table I. When considering the relative volume variations, it appears that the first Li atom entering the *a*-Si core induces a relatively large expansion, whereas only a moderate increase is caused by the Li atoms that follow. This suggests that the *a*-Si core becomes so severely disrupted when the first Li atom enters that it “cracks,” which creates a somewhat open space in the core. The Li atoms that follow can then “fill” this void, resulting in a much smaller volume increase, as is apparent in Fig. 2(b). This is supported by the analysis of the Si-Si coordination in Fig. 2(c), which reveals that the transition leads to a shift towards higher coordination. From the extracted distributions it can be concluded that the

TABLE I. Volume of the lithiated NC_{55} in Å^3 , expansion in percent as compared with the pristine form, and average charge in e^+ for increasing lithiation levels. The difference in the total charge of Li and Si subsystems comes from the fact that a finite part of the electron density is assigned to vacuum in the Bader analysis due to the large surface-to-volume ratio.

Li [number]	Volume [Å^3]	Q_{Si}	Q_{Li}
1	1126 (1.2%)	-0.01	0.85
27	1522 (36.8%)	-0.36	0.83
55	1918 (72.4%)	-0.80	0.81
110	2736 (145.9%)	-1.57	0.79
165	3658 (228.7%)	-2.25	0.75

penetrating Li ion squeezes itself into the surface and compresses the neighbor Si atoms, which explains the observed increase in fivefold coordinated Si atoms. At the same time the number of lower-coordinated Si atoms decreases.

B. Structural changes

The focus is now redirected towards the transformation of the *a*-Si NC₅₅ upon lithiation. Ongoing local structural changes in the *a*-Si structure as a function of the lithiation level are tracked by determining the Si-Si coordination, as shown in Fig. 3. From this plot it can be deduced that the *a*-Si NC undergoes significant changes during lithiation. In its pristine state, the *a*-Si core is characterized by a dense bonding network with a significant proportion of over-coordinated atoms. This is a consequence of the strong confinement occurring in ultrascaled structures. As the cluster surface is progressively saturated, from 1 to 27 Li atoms, there is a continuous transition towards lower coordination and the cluster begins to resemble a piece of bulk *a*-Si. In the phase where Li atoms penetrate into the *a*-Si core, from 27 Li atoms and upwards, the Si coordination continues to decrease. At 55 Li, the *a*-Si network is still partly capable of accommodating the undergoing changes and only one Si atom has a single Si neighbor, whereas the highest frequency in the distribution now corresponds to a coordination of three. However, the Si network gradually deconstructs at higher Li levels, which is clear from the increasing occurrence of Si atoms with coordinations equal to two and one. This is in accordance with previous investigations [24].

To provide more details, the average shortest distances between Li-Li, Li-Si, and Si-Si pairs are also reported in Fig. 3. At low lithiation levels, Li atoms reside on the NC surface, and the distance between Li is large. Furthermore, the Si atoms are not perturbed by the Li atoms and their shortest separation is almost equal to the bulk *a*-Si nearest-neighbor distance. At higher lithiation levels, the shortest pair distances for all combinations of species converge toward 2.55–2.60 Å. These values compare fairly well to 2.62 and 2.65 Å, the Si-Li and Li-Li nearest-neighbor distances in bulk Si₄Li₁₅, respectively [39]. In the case of Si-Si, a distance of 2.55–2.60 Å indicates an increasing number of isolated stretched Si-Si dimers. Note that the variations of the shortest pair distances are smooth, without any abrupt changes or fluctuations when the first Li atom enters into the NC. Moreover, the strong reduction in the variance of the average Li-Li shortest separation provides strong evidence that a transformation toward a homogeneous distribution of the Li atoms takes place in the system.

It should be noted that no sign of fracture is seen during the simulated lithiation process. This suggests that the silicon network is able to handle the resulting large-volume expansion taking place at the inspected NC sizes.

However, in the current work it is only a single lithiation cycle, the first one, that is modeled, whereas repeated (de)lithiation processes should be undertaken and simulations over a larger time scale are required to draw definitive conclusions.

C. Charge transfer

Finally, we examine the charge transfer and localization during lithiation. The resulting charge distributions for three lithiation states are represented as histograms in Fig. 3, with their average values listed in Table I, and shown in Fig. 4. When only one single Li atom resides on the NC surface, one finds a charge transfer of $0.85e^-$ from Li to Si. The fact that Li atoms partly donate their valence electron to the Si atoms is well known for Li/Si systems [40]. However, it is noteworthy that this charge is not carried by nearby surface Si atoms. Instead, it is delocalized over the full Si network. This behavior is different from bulk *c*-Si [22], where the charge transfer has a local character. As lithiation continues, the average charge transferred from Li to Si atoms shows a continuous decrease and reaches $0.78e^-$ for 165 Li. This is consistent with an earlier computational work, where the transfer from Li to bulk *a*-Si is determined to be 0.7 [41]. Interestingly, there is no significant change in the charge distribution and localization when the lithiation threshold is reached and the first Li atom penetrates into a subsurface site. The delocalized charge transfer might explain why the observed bond weakening seen in *c*-Si does not happen in the *a*-Si NCs studied here. In fact, for the NC₅₅ carrying 27 Li atoms, the four most charged Si atoms reside on the surface, whereas the fifth is within the core and none of these are in the vicinity of the Li atom that enters into a subsurface site. At the highest lithiation levels, the negative charge carried by Si atoms increases, as well as the spread of the distribution, from -3.1 to $-1.0e^+$. This is in strong contrast to the Li atoms, which are characterized by a narrow and homogeneous distribution with range of 0.74 to $0.82e^+$. A peculiar consequence of the observed charge transfer is that

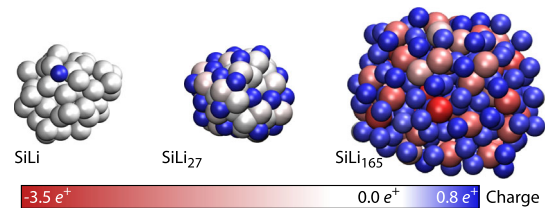


FIG. 4. Charge distribution for NC₅₅ with either 1, 27, or 165 Li atoms in spacefill representation. Small spheres represent Li, whereas large are Si. It is striking that the spread in charge on the Li atoms (blue shades) is insignificant as compared to the Si atoms (red shades). This is also apparent in Fig. 3. Furthermore, the full Si network appears to carry the charge transferred from the Li atoms rather than forming a local buildup of charge on the Si atoms that neighbors Li.

a lithiated system should behave as a dipole with a positive surface and negatively charged center before the critical Li level is reached. Furthermore, an incoming positively charged Li ion will also be repelled by the charged surface Li atoms that have transferred part of their valence charge to the core Si atoms.

D. Transition in site preference

Combining the results from the thermodynamic study and the continuous lithiation processes, one sees that Li atoms first accumulate on the NC surface until a critical coverage is reached. In a second distinct phase they start to penetrate into the NC core. This picture bears similarities with the experimental observation of a Li front and of a two-phase lithiation process at larger system sizes [42–44]. In those configurations, it is currently assumed that Si–Si bond breaking is the rate-limiting event for the displacement of the front, which is promoted by two bond-weakening mechanisms at the interface: (1) charge transfer from the Li atoms that fills Si-Si antibonding levels [40] and (2) tensile strains between lithiated and nonlithiated phase [6]. In the present study, the latter effect can be discarded because the NC surface is free to relax for the relevant Li coverage. Furthermore, the analysis of the charge distribution reveals that the electrons donated by Li atoms are not localized on the surface Si atoms, but rather tend to be homogeneously distributed over the entire *a*-Si core. It is therefore questionable whether charge transfer and the filling of antibonding levels is responsible for the transition occurring at a critical Li coverage in *a*-Si NCs.

We rather propose an alternative mechanism to play the leading role for the lithiation of *a*-Si NCs. Because of charge transfer, Li atoms at the surface become positively charged ions. As a first approximation they can be treated as point charges that repel each other and prefer staying as far apart from each other as possible. At low Li coverage the point charges are able to more or less distribute themselves freely on the surface of the *a*-Si core and maximize the distance to neighboring Li ions. However, as the Li concentration grows they are forced closer to each other, thus increasing the Coulomb repulsion forces. This trend continues up to the point where the repulsion exceeds the cost of breaking up the underlying *a*-Si bond network. When this critical point is reached it becomes energetically favorable for a single Li ion to enter a subsurface site to extend its separation to the neighboring surface Li ions. We propose that this mechanism governs the lithiation of NCs, which is significantly different from what happens in bulk.

Further examinations are required to validate this hypothesis. For that purpose, the influence of the Li ions that surround the first one that enters a subsurface site is investigated by recomputing the previously described NEB runs with slightly different initial and final configurations. Above the thermodynamical threshold the removal of a

neighbor surface Li atom reduces the energy gained by the system when the subsurface site becomes occupied. At this reduced Li level (26 Li) the embedded site is only favored by 0.13 eV, which should be compared to 0.54 eV for the oversaturated surface (27 Li). An even more dramatic change can be achieved if one of the other neighboring Li atoms is removed instead. In this case the subsurface site completely loses its stability and the embedded Li atom falls back to a surface site, leaving a clean *a*-Si core behind. A complete picture is obtained by conducting a similar study for a lithiation level well below the thermodynamical threshold, e.g., 20 Li. In that case, the difference in configuration energy and energy barrier for Li insertion remains more or less unchanged. This picture holds true irrespective of which neighboring Li surface atom is removed (19 Li). These findings are fully consistent with the lithiation mechanism proposed here. In fact, just above the coverage threshold, the surface Li atoms are so close to each other that they strongly interact. Consequently, the removal of one single Li atom drastically affects the energy landscape and the dynamics of the Li atom penetrating into the *a*-Si NC core. Conversely, well below the threshold, the surface Li atoms are separated enough, for their repulsive interaction remains weak and the presence of one more or one less Li atom has no influence.

V. CONCLUSION

From an extensive set of thorough first-principles molecular-dynamics DFT simulations, we have investigated how the lithiation of *a*-Si nanoclusters occurs by determining energy, structural changes, and charge transfer during this process. The collected data enable us to propose the following lithiation scenario: initially Li atoms are found to prefer staying on the surface of the *a*-Si NC. As the lithiation continues, a saturated state is reached, at which the NC surface is fully covered. During this first phase, there is a charge transfer of approximately $0.8e^-$ per Li atom to the Si network. The captured charge is delocalized and spread over the whole *a*-Si NC. Beside an increasing repulsive electrostatic repulsion between the charged Li ions, a structural transformation of the Si network takes place from an over- to a fourfold-coordinated and bulklike state. As lithiation continues, it becomes energetically favorable for one Li atom to penetrate into the *a*-Si NC core. The main driving force for this transition is attributed to the increase in electrostatic repulsion as positively charged Li ions get into a close proximity of each other. This mechanism is different from bulk where a well-defined lithiation front forms enabling the surrounding Si network to screen the Li ions and the weakening of Si–Si bonds as antibonding states are filled is assumed to play a key role. Furthermore, the stress present at the interface between the lithiated and nonlithiated phases that is present in bulk is assumed to promote the movement of the front. However, such stresses do not exist at the *a*-Si NC surface.

We have also found that the Li threshold scales with the size of the NC, and more precisely with its surface, but our restricted set of systems does not permit us to establish a quantitative relation between size and the threshold level.

Once an initial Li atom penetrates beneath the NC surface, we demonstrate that for any additional captured Li further subsurface sites are being occupied with no additional activation-energy barrier. This second lithiation phase is accompanied with significant structural changes of the NC, as exemplified by the Si-Si coordination going from an average of four at the threshold, to 1–2 at a 300% lithiation. The distances between the different species clearly indicate the formation of a lithiated phase, characterized by small fragments of bound Si atoms surrounded by Li atoms. At the maximum lithiation level inspected here, the NC keeps its quasispherical shape.

Finally, the obtained results show that the binding energy steadily decreases from 0.5 to 0.3 eV after the critical lithiation level is surpassed. Within this range of operation the absolute volume expansion per Li atom is determined to be approximately 15 \AA^3 . From this general behavior it seems reasonable to expect that similar characteristics pertain even at higher lithiation levels. These results suggest that the *a*-Si electrode has reached a relatively steady state and it would be favorable to operate it in this regime, whereas a complete Li retraction of the anode electrode should be prevented.

ACKNOWLEDGMENTS

This work was supported by the European Research Council under Grant Agreement No. 335684-E-MOBILE, by the Germaine de Staël program, and by grants from the Swiss Nation Supercomputing Center under Projects No. s579 and No. s666.

-
- [1] Yoshio Idota, Tin-based amorphous oxide: A high-capacity lithium-ion-storage material, *Science* **276**, 1395 (1997).
- [2] M. N. Obrovac, Leif Christensen, Dinh Ba Le, and Jeff R. Dahn, Alloy design for lithium-ion battery anodes, *J. Electrochem. Soc.* **154**, A849 (2007).
- [3] W. J. Zhang, A review of the electrochemical performance of alloy anodes for lithium-ion batteries, *J. Power Sources* **196**, 13 (2011).
- [4] Andreas Pedersen and Mathieu Luisier, Lithiation of tin oxide: A computational study, *ACS Appl. Mater. Interfaces* **6**, 22257 (2014).
- [5] Andreas Pedersen, Petr A. Khomyakov, and Mathieu Luisier, Three-Phase Model for the Reversible Lithiation-Delithiation of SnO Anodes in Li-Ion Batteries, *Phys. Rev. Applied* **4**, 034005 (2015).
- [6] Matthew T. McDowell, Seok Woo Lee, William D. Nix, and Yi Cui, 25th anniversary article: Understanding the lithiation of silicon and other alloying anodes for lithium-ion batteries, *Adv. Mater.* **25**, 4966 (2013).
- [7] Candace K. Chan, Hailin Peng, Gao Liu, Kevin McIlwrath, Xiao Feng Zhang, Robert A. Huggins, and Yi Cui, High-performance lithium battery anodes using silicon nanowires, *Nat. Nanotechnol.* **3**, 31 (2008).
- [8] Nian Liu, Zhenda Lu, Jie Zhao, Matthew T. McDowell, Hyun-Wook Lee, Wenting Zhao, and Yi Cui, A pomegranate-inspired nanoscale design for large-volume-change lithium battery anodes, *Nat. Nanotechnol.* **9**, 187 (2014).
- [9] Maziar Ashuri, Qianran He, and Leon L. Shaw, Silicon as a potential anode material for Li-ion batteries: Where size, geometry and structure matter, *Nanoscale* **8**, 74 (2016).
- [10] Ying Wei, Hang Yu, Haitao Li, Hai Ming, Keming Pan, Hui Huang, Yang Liu, and Zhenhui Kang, Liquid-phase plasma synthesis of silicon quantum dots embedded in carbon matrix for lithium battery anodes, *Mater. Res. Bull.* **48**, 4072 (2013).
- [11] N. Liu, K. Huo, M. T. McDowell, J. Zhao, and Y. Cui, Rice husks as a sustainable source of nanostructured silicon for high performance Li-ion battery anodes, *Sci. Rep.* **3**, 1919 (2013).
- [12] Minseong Ko, Sujong Chae, Sookyung Jeong, Pilgun Oh, and Jaephil Cho, Elastic a-silicon nanoparticle backboneed graphene hybrid as a self-compacting anode for high-rate lithium ion batteries, *ACS Nano* **8**, 8591 (2014).
- [13] Renyuan Zhang, Yuanjin Du, Dan Li, Dengke Shen, Jianping Yang, Zaiping Guo, Hua Kun Liu, Ahmed A. Elzatahry, and Dongyuan Zhao, Highly reversible and large lithium storage in mesoporous Si/C nanocomposite anodes with silicon nanoparticles embedded in a carbon framework, *Adv. Mater.* **26**, 6749 (2014).
- [14] Bin Wang, Xianglong Li, Bin Luo, Long Hao, Min Zhou, Xinghao Zhang, Zhuangjun Fan, and Linjie Zhi, Approaching the downsizing limit of silicon for surface-controlled lithium storage, *Adv. Mater.* **27**, 1526 (2015).
- [15] Xiao Hua Liu, Li Zhong, Shan Huang, Scott X. Mao, Ting Zhu, and Jian Yu Huang, Size-dependent fracture of silicon nanoparticles during lithiation, *ACS Nano* **6**, 1522 (2012).
- [16] Matthew T. McDowell, Seok Woo Lee, Justin T. Harris, Brian A. Korgel, Chongmin Wang, William D. Nix, and Yi Cui, *In Situ* TEM of two-phase lithiation of amorphous silicon nanospheres, *Nano Lett.* **13**, 758 (2013).
- [17] Jiang Wei Wang, Yu He, Feifei Fan, Xiao Hua Liu, Shuman Xia, Yang Liu, C. Thomas Harris, Hong Li, Jian Yu Huang, Scott X. Mao, and Ting Zhu, Two-phase electrochemical lithiation in amorphous silicon, *Nano Lett.* **13**, 709 (2013).
- [18] Xiao Hua Liu *et al.*, Anisotropic swelling and fracture of silicon nanowires during lithiation, *Nano Lett.* **11**, 3312 (2011).
- [19] Hui Yang, Shan Huang, Xu Huang, Feifei Fan, Wentao Liang, Xiao Hua Liu, Long-Qing Chen, Jian Yu Huang, Ju Li, Ting Zhu, and Sulin Zhang, Orientation-dependent interfacial mobility governs the anisotropic swelling in lithiated silicon nanowires, *Nano Lett.* **12**, 1953 (2012).
- [20] Payam Kaghazchi, Mechanism of Li intercalation into Si, *Appl. Phys. Lett.* **102**, 093901 (2013).
- [21] Jochen Rohrer, Ashkan Moradabadi, Karsten Albe, and Payam Kaghazchi, On the origin of anisotropic lithiation of silicon, *J. Power Sources* **293**, 221 (2015).

- [22] Kejie Zhao, Wei L Wang, John Gregoire, Matt Pharr, Zhiqiang Suo, Joost J Vlassak, and Efthimios Kaxiras, Lithium-assisted plastic deformation of silicon electrodes in lithium-ion batteries: A first-principles theoretical study, *Nano Lett.* **11**, 2962 (2011).
- [23] Priya Johari, Yue Qi, and Vivek B Shenoy, The mixing mechanism during lithiation of Si negative electrode in Li-ion batteries: An *ab initio* molecular dynamics study, *Nano Lett.* **11**, 5494 (2011).
- [24] Ekin D. Cubuk and Efthimios Kaxiras, Theory of structural transformation in lithiated amorphous silicon, *Nano Lett.* **14**, 4065 (2014).
- [25] Y. Okamoto, Dynamical aspects of lithiation of a nanosized silicon cluster, *J. Phys. Chem. C* **115**, 25160 (2011).
- [26] G. Kresse and J. Furthmüller, Efficient iterative schemes for *ab initio* total-energy calculations using a plane-wave basis set, *Phys. Rev. B* **54**, 11169 (1996).
- [27] G. Kresse and J. Furthmüller, Efficiency of *ab-initio* total energy calculations for metals and semiconductors using a plane-wave basis set, *Comput. Mater. Sci.* **6**, 15 (1996).
- [28] P. E. Blöchl, Projector augmented-wave method, *Phys. Rev. B* **50**, 17953 (1994).
- [29] J. P. Perdew, K. Burke, and M. Ernzerhof, Generalized Gradient Approximation Made Simple, *Phys. Rev. Lett.* **77**, 3865 (1996).
- [30] D. Tománek and M. A. Schlüter, Structure and bonding of small semiconductor clusters, *Phys. Rev. B* **36**, 1208 (1987).
- [31] M. F. Jarrold and V. A. Constant, Silicon Clusters Ions: Evidence for a Structural Transition, *Phys. Rev. Lett.* **67**, 2994 (1991).
- [32] Ian A. Courtney, J. S. Tse, O. Mao, J. Hafner, and Jeff R. Dahn, *Ab initio* calculation of the lithium-tin voltage profile, *Phys. Rev. B* **58**, 15583 (1998).
- [33] V. L. Chevrier and Jeff R. Dahn, First principles model of amorphous silicon lithiation, *J. Electrochem. Soc.* **156**, A454 (2009).
- [34] Maria K. Y. Chan, Chris Wolverton, and Jeffrey P. Greeley, First principles simulations of the electrochemical lithiation and delithiation of faceted crystalline silicon, *J. Am. Chem. Soc.* **134**, 14362 (2012).
- [35] Graeme Henkelman, Blas Uberuaga, and Hannes Jónsson, A climbing image nudged elastic band method for finding saddle points and minimum energy paths, *J. Chem. Phys.* **113**, 9901 (2000).
- [36] Søren Smidstrup, Andreas Pedersen, Kurt Stokbro, and Hannes Jónsson, Improved initial guess for minimum energy path calculations, *J. Chem. Phys.* **140**, 214106 (2014).
- [37] A. Pedersen, L. Pizzagalli, and H. Jónsson, Optimal atomic structure of amorphous silicon obtained from density functional theory calculations (to be published).
- [38] Graeme Henkelman, Andri Arnaldsson, and Hannes Jónsson, A fast and robust algorithm for bader decomposition of charge density, *Comput. Mater. Sci.* **36**, 354 (2006).
- [39] Yoshiyuki Kubota, Mary Clare Sison Esgañó, Hiroshi Nakanishi, and Hideaki Kasai, Crystal and electronic structure of $\text{Li}_{15}\text{Si}_4$, *J. Appl. Phys.* **102**, 053704 (2007).
- [40] Hyunwoo Kim, Kyoung Eun Kweon, Chia-Yun Chou, John G. Ekerdt, and Gyeong S. Hwang, On the nature and behavior of Li atoms in Si: A first principles study, *J. Phys. Chem. C* **114**, 17942 (2010).
- [41] V. L. Chevrier and Jeff R. Dahn, First principles studies of disordered lithiated silicon, *J. Electrochem. Soc.* **157**, A392 (2010).
- [42] Matthew T. McDowell, Ill Ryu, Seok Woo Lee, Chongmin Wang, William D. Nix, and Yi Cui, Studying the kinetics of crystalline silicon nanoparticle lithiation with *in situ* transmission electron microscopy, *Adv. Mater.* **24**, 6034 (2012).
- [43] Matthew T McDowell, Seok Woo Lee, Justin T Harris, Brian A Korgel, Chongmin Wang, William D Nix, and Yi Cui, *In situ* TEM of two-phase lithiation of amorphous silicon nanospheres, *Nano Lett.* **13**, 758 (2013).
- [44] Jiang Wei Wang, Yu He, Feifei Fan, Xiao Hua Liu, Shuman Xia, Yang Liu, C Thomas Harris, Hong Li, Jian Yu Huang, Scott X Mao, and Ting Zhu, Two-phase electrochemical lithiation in amorphous silicon, *Nano Lett.* **13**, 709 (2013).